

Performance of stainless steel welded beam-column joint under cyclic loading

A. Nayeem & S. Ahmed

Bangladesh University of Engineering and Technology, Dhaka 1000, Bangladesh

ABSTRACT: Now a days, stainless steel is being increasingly used in construction industries. It is characterized by its nonlinear stress-strain behavior with significant strain hardening. Being a highly ductile material, stainless steel structures may demonstrate better seismic resistance than traditional carbon steel structures. Seismic performance of a steel structure depends on the behavior of its beam-column joint under cyclic loading. But very limited researches were found on stainless steel joints. The current paper numerically investigates the performance of stainless steel beam-column joint under cyclic loading. For this, a numerical model of beam-column connection of carbon steel was developed and verified for cyclic loading. Later, the material properties of the verified model were replaced by the equivalent properties of stainless steel to get the behavior of stainless steel joints for SAC 1997, FEMA 461 and Near Fault cyclic loading protocols. The performance was evaluated on the basis of ultimate moment capacity, energy dissipation and residual moment capacity of the joint. The comparison showed that stainless steel beam-column dissipated more energy than carbon steel joint for all three cyclic loading protocols. The ultimate moment capacity and residual moment capacity after cyclic loading of stainless steel joint were also higher than those of carbon steel joint.

1 INTRODUCTION

Recently stainless steel (SS) has received increasing attention as construction material for its corrosion resistance behavior and low maintenance cost. It is also pleasant in appearance, highly ductile and performs better in fire (Gardner 2005, Baddo 2008, Gedge 2008 and Rossi 2014). The mechanical behavior of stainless steel is significantly different from that of Carbon steel. Stainless steel exhibits rounded stress strain curve with no definite yield point and shows significantly higher strain hardening. Moreover, stainless steel is more ductile than carbon steel, particularly in the case of the austenitic and duplex grades. The percentage elongation values at fracture for stainless steel is between 40–60% and values of ultimate-to-yield strength ratios typically around 1.5–2.0. A number of design codes are currently available for stainless steel such as SEI/ASCE-8-02 (2002), AS/NZS 4673 (2001) and EN, 1993-1-4 (2006). However, due to insufficient studies, all available codes do not provide sufficient details on joint design.

Among the previous researchers, Errera et al. (1974) first reported the capacity of bolted and welded stainless steel connections. Later Ryan (1999) performed some tests on thick stainless steel bolted connection. Kim and Kuwamura (2007) numerically investigated bolted connections between cold-formed stainless steel sheets. Bouchair et al. (2008) studied the behavior of stainless steel lap joint connections experimentally and numerically. Kiyamaz (2009) investigated the bearing strength of stainless steel bolted plates under in-plane tension. Salih et al. (2010 and 2011) studied the net cross-section failure and the bearing failure of bolted lap joints for different grades of stainless steel. They also studied the behavior of stainless gusset plate connections (Salih et al. 2013). All the aforementioned studies concentrated mainly on the behavior of bolted connection between two plates. Recently, Elflah et al. (2018) and Hasan et al. (2019) observed the moment rotation behavior of semi-rigid beam-column joint by testing full scale specimens. However, the performance of stainless steel beam-column joints under cyclic loading is still subjected to study. The cyclic behavior of beam-column joints plays important rule to evaluate the seismic performance of stainless steel structures. Furthermore, there is no evidence on the behavior of welded beam-column joints of stainless steel.

The intend of this study is to numerically explore the performance of stainless steel welded beam-column joint under cyclic loading. For this reason, a finite element (FE) model was developed where an I-beam was

connected to a box column. Initially, the developed model was validated against with experimental result of carbon steel beam-column joints due to the lake of experimental results on stainless steel joint. Using the validated model, the behavior of stainless steel joints was studied for three different cyclic loading protocol. Finally, the performance of stainless steel joint was compared with carbon steel joint.

2 FE MODELING

In this study, a beam-column joint of carbon steel was model using commercial finite element analysis package ABAQUS (2014). In this joint an I-beam (I-380×200×8×12 mm) was connected to a square hollow column (B-400×400×20×20 mm) with flange plates and a shear tab. The dimensions of the joint were taken from the experiment performed by Gholami et al. (2013). The height of the column was 3000 mm and the beam was 2520 mm long from the column edge. The top flange plate was 300 mm long and 20 mm thick and bottom flange plate was 300 mm long and 15 mm thick. Beam was welded to the flange plates and then flange plates were welded to the column. Continuity plates of 20 mm thickness for top and 15 mm thickness for bottom were also welded inside the column at the locations where flange plates were connected. The details of the joint are shown in Figure 1.

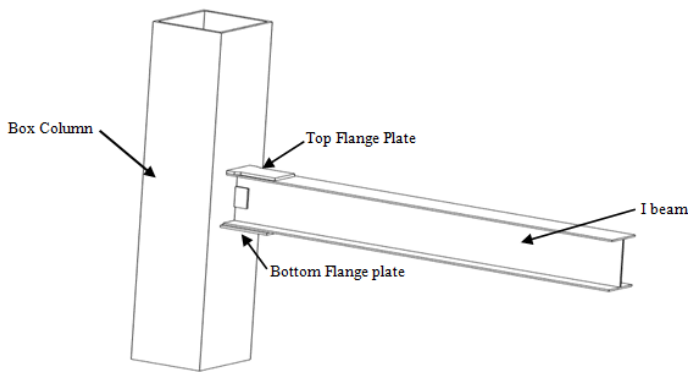


Figure 1. Schematic diagram of the beam-column joint.

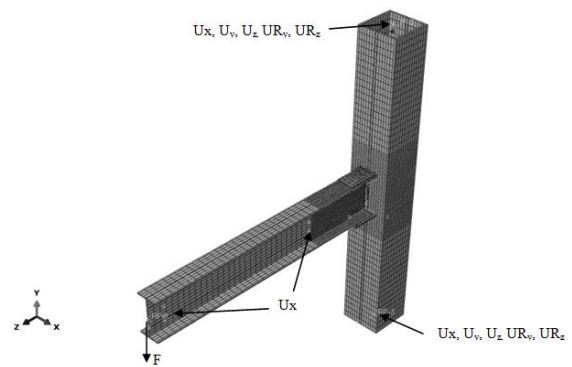


Figure 2. Mesh distribution and support condition of beam-column joint model.

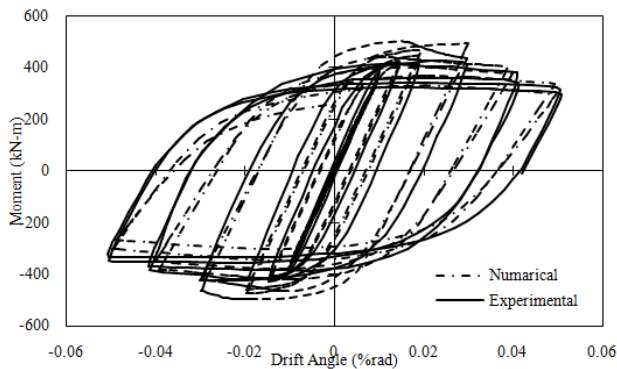
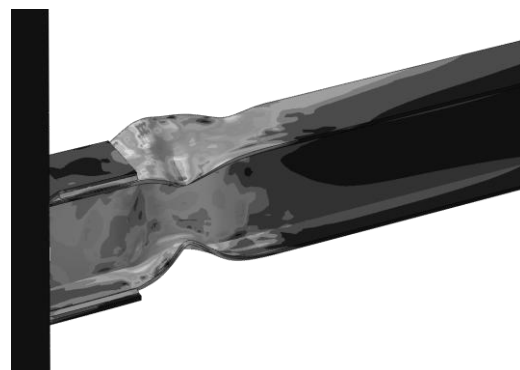


Figure 3. Comparison of hysteresis loops of experimental result and numerical analysis of the beam-column joint.



(a) Experimental deformed shape.



(b) Numerical deformed shape.

Figure 4. Deformed shapes of the beam-column joint.

The model was developed using solid elements. 20-noded quadratic brick element (C3D20R) was used to model all the components of the joints i.e. beam, column, flange plates, shear tab and welds. Variable mesh sizes were adopted in the model to achieve a reliable result at a reasonable computational time. Mesh sizes varied from 10 mm to 40 mm. Relatively finer mesh was assigned near the region of beam-column joint where large deformation and distortion of elements were expected. Relatively coarser mesh was assigned in other regions. Bilinear stress strain relationship was used for carbon steel and weld material. All material properties of beam, column, flange plates and weld materials were incorporated from the experiment (Gholami et al. 2013). In the experiment, column was pin connected at both the ends. To simulated the support condition, all the nodes of each ends were coupled with reference points at the center of the respective sections. All translations and rotations of the reference points were restrained except the rotation about the bending axis (x-axis in Fig-2.2). Lateral supports were provided by restraining translation along x-axis at 700 mm and 2300 mm of the beam to prevent lateral-torsional buckling. Load was applied at the tip of the beam as a displacement following the cyclic loading protocol SAC 1997. The mesh distribution and support conditions of the model are shown in Figure 2.

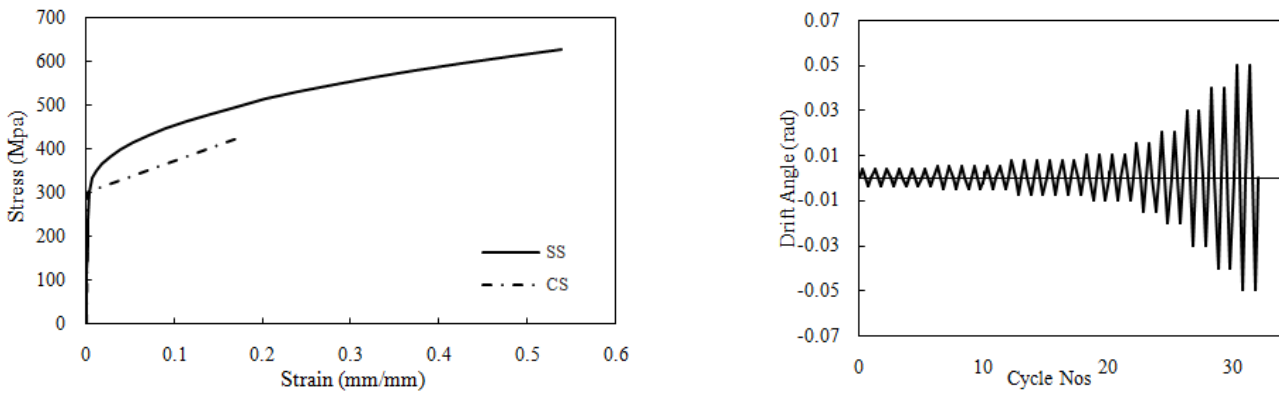
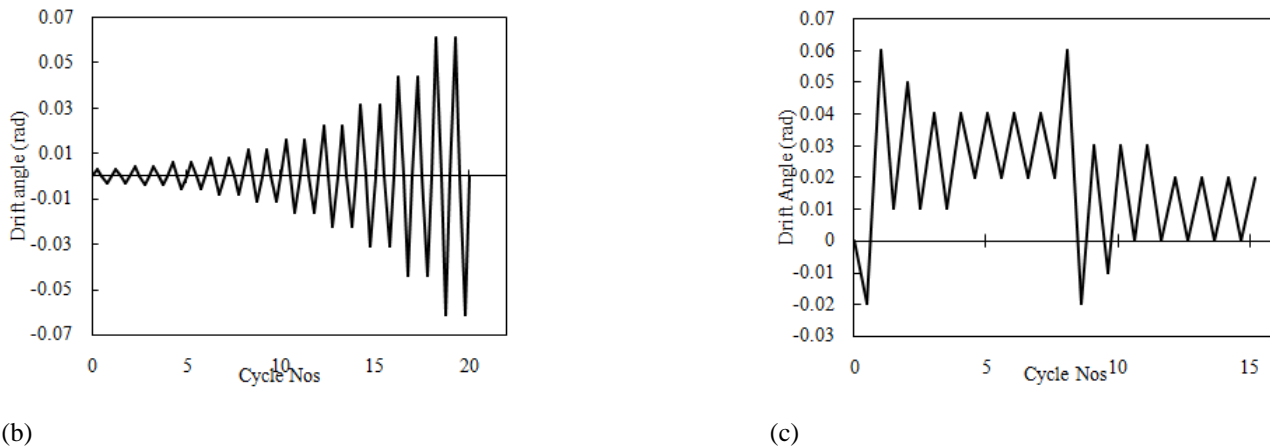


Figure 5. Stress strain relationship of carbon steel and stainless steel. (a)



(b) (c)
Figure 6. Different cyclic loading protocol (a) SAC-1997 (b) FEMA 461 (c) Near fault.

3 VERIFICATION OF FE MODEL

The performance of the finite element model developed here was evaluated by comparing the results of FE analysis with the experiment result of Gholami et al. (2013). Moment-rotation behavior, energy dissipation as well as deformation shape were considered here. Moment at column face versus drift angle from FE analysis and experimental investigation were presented in Figure 3. It is observed that the hysteresis loops of FE analysis and experimental result are very similar. The energy dissipation of a joint is the area of the hysteresis loop of moment-drift angle. The energy dissipation values of the joint calculated from the FE analysis and experimental results were 262 and 250 kilo-Joule respectively. So, the variation in energy dissipation is only 3.7%. Figures 4 (a) and (b) illustrate the deflected shapes of the joint obtained from experiment and analysis. The deflected shapes show that they are identical in nature. In the comparison, it is clear that the FE model is able to simulate the behavior of beam-column joint with good accuracy. Therefore, this model can be used for evaluating the seismic performance beam-column joints in the following sections.

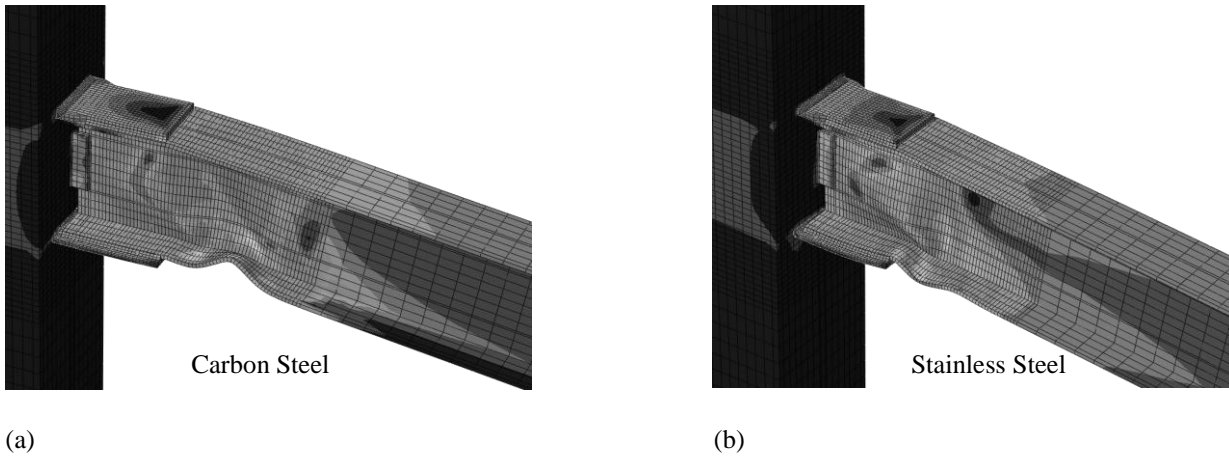


Figure 7. Deformed shapes of (a) carbon steel and (b) stainless steel beam-column joints under monotonic load.

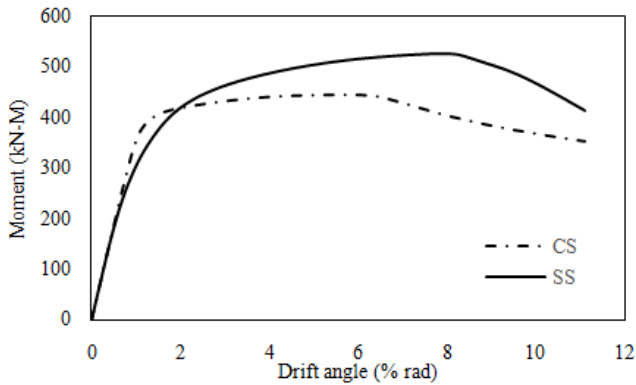


Figure 8. Moment vs. drift angle of carbon steel and stainless steel beam-column joints for monotonic loading.

4 STAINLESS STEEL JOINT AND LOADS

The beam-column joint model validated in the previous section was used to evaluate the performance of stainless steel beam-column joint. Later, the behavior of stainless steel joint was compared with carbon steel joint. To make the comparison easier, carbon steel and stainless steel grades was chosen conscientiously. For this purpose, both the materials have the same yield stress of 300 MPa. For carbon steel the ultimate strength was 430 MPa according to Gholami et al. (2013). The ultimate strength of stainless steel was calculated from the correlation proposed by Rasmussen (Arrayagoa et al. 2015) and the value was 628 MPa. Bilinear material stress strain was adopted for carbon steel. However, modified Rasmussen model (Arrayagoa et al. 2015) has been considered for stress strain relationship of stainless steel. The material properties of weld material remained same as used in the experiment (Gholami et al. 2013) for both the models. Stress strain relationship of carbon steel and stainless steel are shown in Figure 5.

There are different loading protocols to assess the seismic performance of structural elements. For steel joints SAC 1997 (Clark et al., 1997), FEMA 461 and Near Fault Protocol (Krawinkler et al. 2000) are the most commonly used cyclic loading protocols. The target maximum drift amplitude was considered 0.05 rad for SAC 1997 and 0.06 rad for FEMA 461 protocols. The SAC protocol contains more small elastic cycles. In Near Fault protocol, the maximum drift amplitude was 0.06 rad with a pulse reversal in its loading history. Figure 6 represents the cyclic loading protocols. Both the models of stainless steel and carbon steel joints were analyzed with these three loading protocols individually to observed the behavior of the beam-column joints. Along with the cyclic loadings, behavior of the joints was also analyzed for monotonic loading.

5 PERFORMANCE OF STAINLESS STEEL JOINT

In this section, the behavior of stainless steel joint was compared with carbon steel joint based on their ultimate moment capacity, energy dissipation and deflected shapes. Figures 7 and 8 show the deflected shapes and the moment vs. drift angle curve for monotonic load for stainless steel and carbon steel joints respectively. It is observed that, the deflections of both the joints are similar. In both cases bottom flange buckled. For SS joint bottom plate buckled just after the flange plates. However, in case of CS joint, buckling happed a little

bit away from the nose of the bottom flange plate. From the moment rotation curves it is found that stainless steel joint loses stiffness in early stage than carbon steel joint. But the ultimate moment capacity of stainless steel joint was much higher than carbon steel joints. Ultimate moment capacity of SS joint is 525 kN-m, which is 18% higher than that of CS joint. The deformability (rotation at ultimate load) of SS joint is also higher than CS joint. This behavior is desirable as stainless steel shows early nonlinearity and has significant strain hardening property.

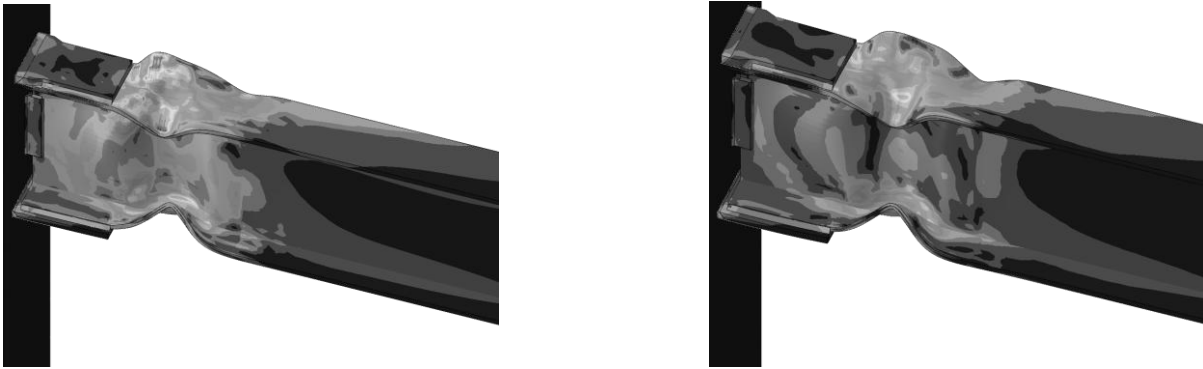


Figure 9. Deformed shapes of carbon steel and stainless beam-column joints for SAC 1997 cyclic loading protocol.

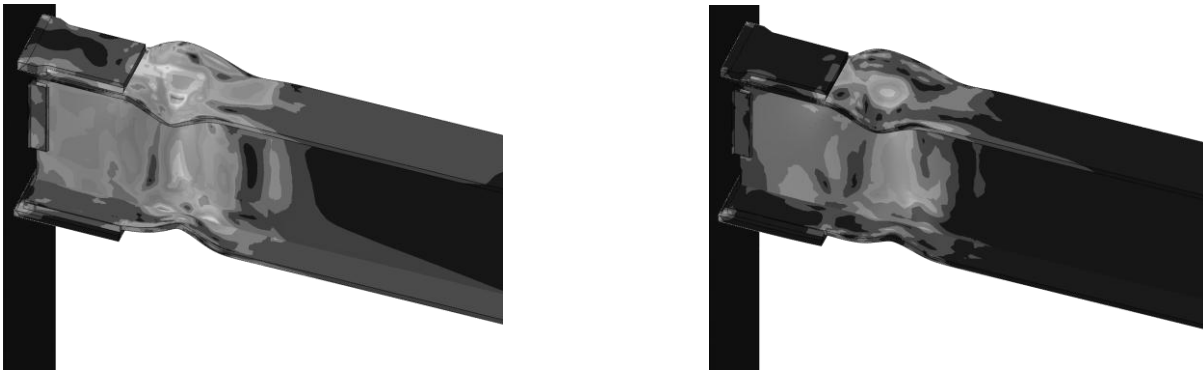


Figure 10. Deformed shapes of carbon steel and stainless steel beam-column joints for near fault cyclic loading protocol.

Behavior of stainless steel joint under cyclic load was investigated for three different loading protocols. Figure 9 shows the deform shape of SS joint and CS joint for SAC 1997 loading protocol. Both the joints deformed very similarly in the way of forming plastic hinges. In both the cases, yielding was initiated in the beam flange at the nose of the flange and gradually propagated towards the mid span. The lengths of the plastic hinge regions for SS joint and CS joint were almost same, 385 mm and 388 mm respectively. Similar comparison was found for FEMA 461 load. For near fault loading protocol, SS joint and CS joint deformed in similar nature but their plastic hinge regions were much smaller. The deform shapes of SS joint and CS joint for near fault loading protocol are shown in Figure 10.

Moment at column face versus drift angle hysteresis loop has been plotted in Figure 11 to 13 to compare the performance of SS joint and CS joint under cyclic load for all three loading protocols: SAC 1997, FEMA 461 and Near Fault. Figure 14 also presents the comparison of energy dissipation of the joints. The comparison shows that SS joint dissipated more energy than CS joint for all cases. The reason for results is that strain hardening strength of SS is much higher than that of CS. For SAC 1997, SS joint dissipated 10% more energy than CS joint. Having higher maximum amplitude, for FEMA 461 energy dissipation of SS joint was 12% higher than CS joint. In near fault loading protocol, amplitudes of most of the cycles are relatively small. As a result, energy dissipation of SS joint and CS joint was low and they were very close.

The residual moment capacities of SS joint and CS joint were also determined for the comparison. For this purpose, a monotonic load was applied to determine the moment capacity after application of cyclic load. In Figure 15, the residual moment capacities of SS joint and CS joint were presented after applying all three cyclic loading protocols considered here. It found that the residual capacities of SS joint were higher than those of CS joint for all the cases. The residual capacities SS joint were 90%, 85% and 94% of the initial ultimate moment capacity for SAC 1997, FEMA 461 and Near Fault loading protocols respectively. However, these values were 75%, 69% and 86% for CS joint.

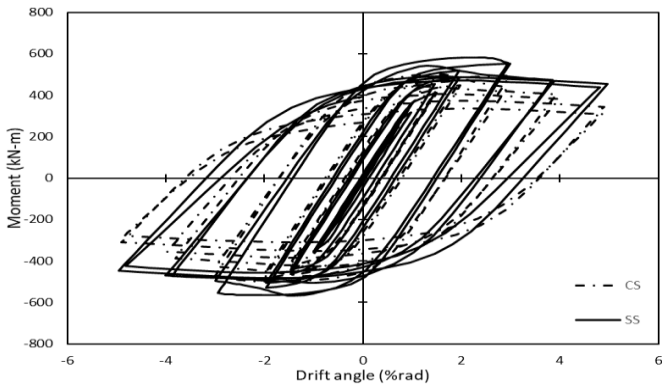


Figure 11. Hysteresis loops of carbon steel and stainless steel beam-column joints for SAC 1997 cyclic loading protocol.

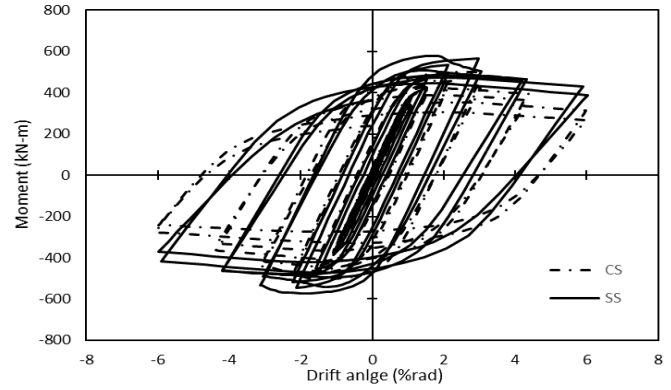


Figure 12. Hysteresis loops of carbon steel and stainless steel beam-column joints for FEMA-461 cyclic loading protocol.

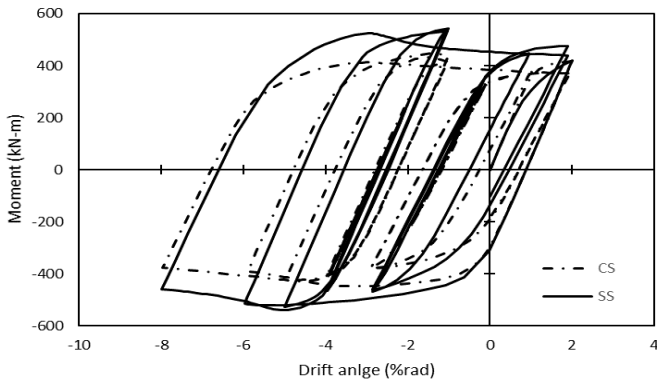


Figure 13. Hysteresis loops of carbon steel and stainless steel beam-column joints for near fault cyclic loading protocol.

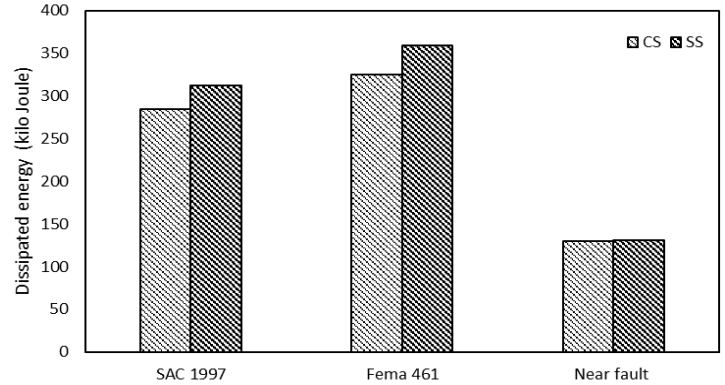


Figure 14. Comparison of dissipated energy of carbon steel and stainless steel beam-column joints for different loading protocols.

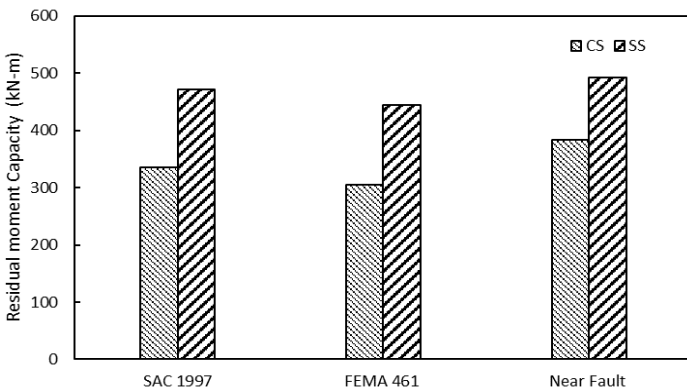


Figure 15. Residual moment capacity of carbon steel and stainless steel beam-column joints for different loading protocols.

6 CONCLUSIONS

In this paper, the performance of the stainless steel joint under cyclic loading was evaluated on the basis of finite element analysis. For this purpose, a FE model of a welded beam-column joint of I-beam and the square hollow column was developed and validated against experimental results. Using this model, the behavior of the SS joint was assessed and compared with CS joint for monotonic load and cyclic load. Ultimate moment capacity of the SS joint was 18% higher than that of the CS joint. Both SS joint and CS joint were analyzed for SAC 1997, FEMA 461, and Near Fault cyclic loading protocols. In all the cases, deformation shapes of the SS joint and CS joint were very similar. From hysteresis loops, dissipated energy was calculated. It was observed that, due to higher strain-hardening strength, SS joint dissipated more energy than CS joint under cyclic loading. With the increase of the amplitudes of loading protocols, the ratio of dissipated energy between SS joint and CS joint increases. The residual capacity of the SS joint after cyclic loading was also significantly higher than CS joint.

REFERENCES

- ABAQUS, 2014. ABAQUS User's Manual v6.14, Dassault Systèmes Simulia Corp, Providence, RI, USA.
- Arrayagoa, I. Reala, E. & Gardner, L. 2015. Description of stress-strain curves for stainless steel alloys. *Materials & Design* 87:540-552.
- AS/NZS 4673. 2001. Australian/New Zealand Standard (AS/NZS) in Cold-formed stainless steel structures, Standards Australia, Sydney, Australia.
- Baddoo, N.R. 2008. Stainless steel in construction: a review of research, applications, challenges and opportunities, *J. Constr. Steel Res.* 64 (11): 1199-1206.
- Bouchair, A. Averseng, J. & Abidelah, A. 2008. Analysis of the behaviour of stainless steel bolted connections. *J Constr Steel Res* 64(11):1264-74.
- Clark, P. Frank, K. Krawinkler, H. & Shaw, R. 1997. Protocol for Fabrication, Inspection, Testing, and Documentation of Beam-Column Connection Tests and Other Experimental Specimens. SAC Steel Project Background Document. Report No. SAC/BD-97/02.
- Elflah, M. Theofanous, M. Dirar, S. & Yuan, H. 2018. Behaviour of stainless steel beam-to-column joints—Part 1: Experimental investigation. *Journal of Constructional Steel Research* 152:183-193.
- EN 1993-1-4. 2006. Eurocode 3: Design of steel structures - Part 1-4: General rules - Supplementary rules for stainless steels. Brussels: European Committee for Standardization.
- Errera, S.J. Popowich, D.W. & Winter, G. 1974. Bolted and welded stainless steel connections, *J. Struct. Eng.* ASCE 100 (6): 1279-1296.
- FEMA-461. 2007. Interim Protocols for Determining Seismic Performance Characteristics of Structural and Nonstructural Components Through Laboratory Testing. FEMA 461 Draft document, Federal Emergency Management Agency.
- Gardner, L. 2005. The use of stainless steel in structures. *ProgStructEng Mater* 7(2):45-55.
- Gedge, G. 2008. Structural uses of stainless steel - buildings and civil engineering, *J. Constr. Steel Res.* 64 (11): 1194-1198.
- Gholami, M. Deylami, A. & Tehranizadeh, M. 2013. Seismic performance of flange plate connections between steel beams and box columns. *Journal of Constructional Steel Research* 84: 36-48.
- Hasan, M. J. Al-Deen, S. & Ashraf, M. 2019. Behaviour of top-seat double web angle connection produced from austenitic stainless steel. *Journal of Constructional Steel Research* 155: 460-479.
- Kim, T.S. & Kuwamura, H. 2007. Finite element modelling of bolted connections in thin walled stainless steel plates under static shear. *Thin-Walled Struct* 45(4):407-21.
- Kiyamaz, G. 2009. Investigations on the bearing strength of stainless steel bolted plates under in-plane tension. *Steel Compos Struct* 9(2):173-89.
- Krawinkler, H. Gupta, A. Medina, R. & Luco, N. 2000. Development of Loading Histories for Testing of Steel Beam-to-Column Assemblies. SAC Background Report SAC/BD-00/10.
- Rossi, B. 2014. Discussion on the use of stainless steel in constructions in view of sustainability, *Thin-Walled Struct* 83: 182-189.
- Ryan, I. 1999. Development of the Use of Stainless Steel in Construction. WP 4.2 ECSC Project No. 7210-SA/327
- Salih, E.H. Gardner, L. Nethercot, D.A. 2013. Numerical study of stainless steel gusset plate connections, *Eng. Struct* 49: 448-464.
- Salih, E.L. Gardner, L. & Nethercot, D.A. 2010. Numerical investigation of net section failure in stainless steel connections. *J Constr Steel Res* 66(12):1455-66.
- Salih, E.L. Gardner, L. & Nethercot, D.A. 2011. Bearing failure in stainless steel bolted connections. *EngStruct* 33(2):549-62.
- SEI/ASCE-8-02, 2000. Specification for the design of cold-formed stainless steel structural members, American Society of Civil Engineers (ASCE), ASCE Standard, Virginia, USA.